Molecular Therapy
Original Article

Microglial lnc-U90926 facilitates neutrophil infiltration in ischemic stroke via MDH2/CXCL2 axis

Jian Chen,[1,2,3,4,5,6] Jiali Jin,[1,2,3,4,5,6] Xi Zhang,[1,2,3,4,5] Hailong Yu,[1,2,3,4,5] Xiaolei Zhu,[1,2,3,4,5] Linjie Yu,[1,2,3,4,5] Yanting Chen,[1,2,3,4,5] Pinyi Liu,[1,2,3,4,5] Xiaohong Dong,[1,2,3,4,5] Xiang Cao,[1,2,3,4,5] Yue Gu,[1,2,3,4,5] Xinyu Bao,[1,2,3,4,5] Shengnan Xia,[1,2,3,4,5] and Yun Xu[1,2,3,4,5]

[1]Department of Neurology, Drum Tower Hospital, Medical School and The State Key Laboratory of Pharmaceutical Biotechnology, Nanjing University, Nanjing, Jiangsu 210008, P.R. China; [2]Institute of Brain Sciences, Nanjing University, Nanjing, Jiangsu 210093, P.R. China; [3]Jiangsu Key Laboratory for Molecular Medicine, Medical School of Nanjing University, Nanjing, Jiangsu 210008, P.R. China; [4]Jiangsu Province Stroke Center for Diagnosis and Therapy, Nanjing, Jiangsu 210008, P.R. China; [5]Nanjing Neurology Clinic Medical Center, Nanjing, Jiangsu 210008, P.R. China

Dysregulated long non-coding RNAs (lncRNAs) have been shown to contribute to the pathogenesis of ischemic stroke. However, the potential role of lncRNAs in post-stroke microglial activation remains largely unknown. Here, we uncovered that lncRNA-U90926 was significantly increased in microglia exposed to ischemia/reperfusion both *in vivo* and *in vitro*. In addition, adenovirus-associated virus (AAV)-mediated microglial U90926 silencing alleviated neurological deficits and reduced infarct volume in experimental stroke mice. Microglial U90926 knockdown could reduce the infiltration of neutrophils into ischemic lesion site, which might be attributed to the downregulation of C-X-C motif ligand 2 (CXCL2). Mechanistically, U90926 directly bound to malate dehydrogenase 2 (MDH2) and competitively inhibited the binding of MDH2 to the CXCL2 3′ untranslated region (UTR), thus protecting against MDH2-mediated decay of CXCL2 mRNA. Taken together, our study demonstrated that microglial U90926 aggravated ischemic brain injury via facilitating neutrophil infiltration, suggesting that U90926 might be a potential biomarker and therapeutic target for ischemic stroke.

INTRODUCTION

Microglia are the dominant immune cells within the central nervous system (CNS), acting as guardians of the brain, and are found to be the sentinels that first respond to various acute brain injuries, including acute ischemic stroke (AIS).[1,2] After ischemic stroke, microglia immediately migrate toward the lesion site and exacerbate tissue injury via releasing pro-inflammatory cytokines.[1,3] In addition, following inflammatory cytokines and chemokines released by the post-stroke activated microglia, peripheral immune cells, such as neutrophils, T cells, and natural killer (NK) cells, are recruited into the ischemic hemisphere and exert elaborate functions.[4–6] Among the infiltrated immune cells, neutrophil is widely reported to play an important role in determining the outcome of ischemic stroke as a double-edged sword. In the acute phase of post-stroke inflammation, neutrophils are immediately recruited into the ischemic lesion site and exacerbate ischemic injury via damaging neural cells and the integrity of the blood-brain barrier (BBB).[7,8] However, similar to microglia, in the late phase of post-stroke inflammation, neutrophils can also contribute to tissue repair and remodeling via removing necrotic tissue and cellular debris, producing growth factors and proangiogenic factors.[8,9] Because of the detrimental role of microglia and neutrophils in the acute stage of ischemic stroke, manipulating microglial activation and neutrophil infiltration might provide new therapeutic interventions for acute ischemic stroke.[10–12]

Infiltration of neutrophils into the ischemic area initiates only 30 min post-stroke, peaks at 24–48 h, and thereafter declines.[13,14] The migration of neutrophils is a complicated process dependent on abundant molecules and chemokines, during which microglia are widely reported to play an important role because of the chemokines recruiting neutrophils released by microglia, such as CXCL1 and CXCL2,[15,16] although these chemokines could also be released by other cell types, including endothelial cells, fibroblasts, monocytes, and macrophages.[17,18] Thus, microglia hold potential to be a prime therapeutic target for modulating post-stroke neuroinflammation.

Long non-coding RNAs (lncRNAs) are a set of transcripts that are longer than 200 bp and rarely encode functional short peptides.[19,20] lncRNA expression profiles are found to be significantly altered in the serum and brain of stroke patients and mice.[21] Moreover, lncRNAs have been proven to modulate post-stroke microglial activation.[21] lncRNA H19 promotes post-stroke neuroinflammation via

Received 24 October 2020; accepted 19 April 2021;
https://doi.org/10.1016/j.ymthe.2021.04.025.

[6]These authors contributed equally

Correspondence: Yun Xu, MD, PhD, Department of Neurology, Drum Tower Hospital, Medical School and The State Key Laboratory of Pharmaceutical Biotechnology, Nanjing University, 321 Zhongshan Road, Nanjing, Jiangsu 210008, P.R. China.
E-mail: xuyun20042001@aliyun.com

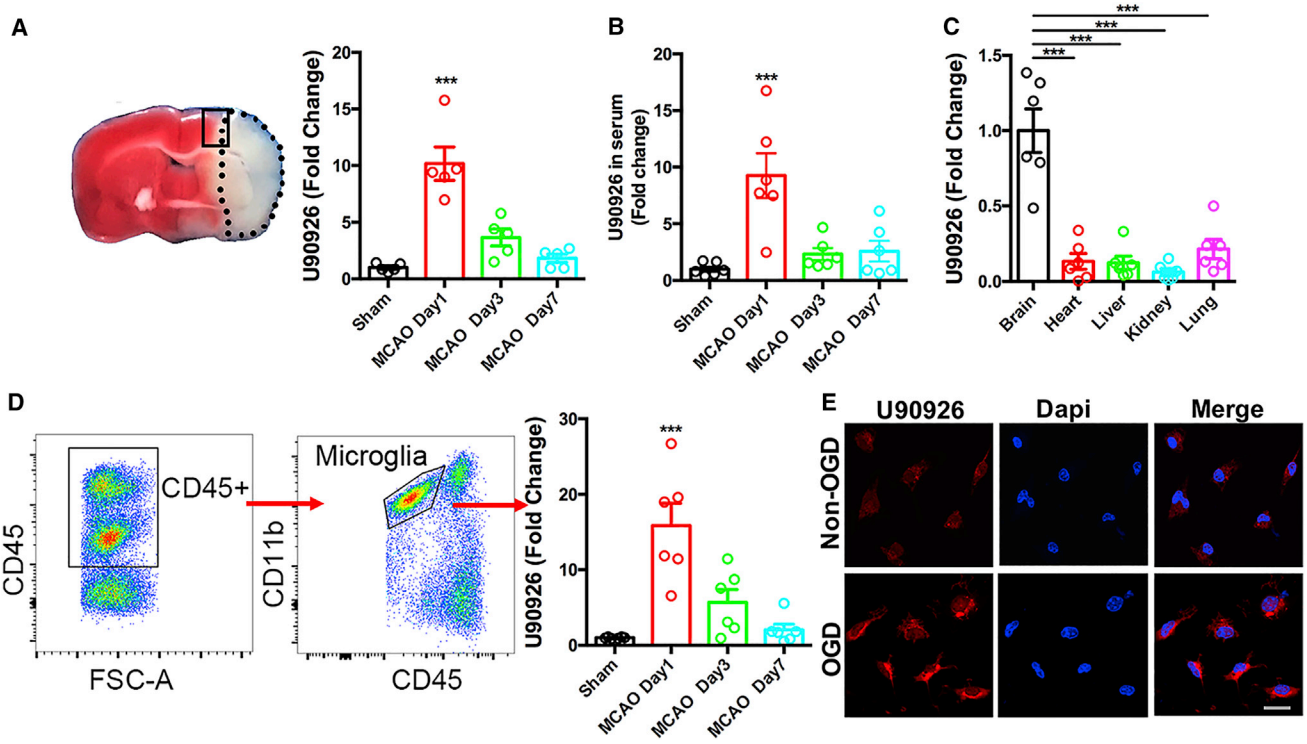

Figure 1. Upregulation of U90926 in microglia after ischemic stroke

(A) U90926 expression level in the ischemic penumbra of tMCAO mice was detected via quantitative real-time PCR. n = 5 mice per group. ***p < 0.001 versus the sham group, one-way ANOVA with Bonferroni post hoc test. (B) U90926 expression level in the serum of tMCAO mice was detected via quantitative real-time PCR. n = 6 mice per group. ***p < 0.001 versus the sham group, one-way ANOVA with Bonferroni post hoc test. (C) U90926 expression levels in different organs (brain, heart, liver, kidney, lung) of tMCAO mice were detected via quantitative real-time PCR. n = 6 mice per group. ***p < 0.001 versus the brain group, one-way ANOVA with Bonferroni post hoc test. (D) Microglia were isolated from the ischemic hemispheres via FACS, and the U90926 level was measured via quantitative real-time PCR. One dot represents 2 mice, n = 12 mice per group. ***p < 0.001 versus the sham group, one-way ANOVA with Bonferroni post hoc test. (E) The localization of U90926 in primary microglia was examined by FISH assay. Scale bar: 20 μm. Data are presented as mean ± SEM; p values are reported in Table S1.

driving histone deacetylase 1-dependent M1 microglial polarization.[22] Our previous study also uncovered that lncRNA 1810034E14Rik reduces post-stroke microglial activation.[23] However, bulk tissue, rather than isolated microglia, was used in most studies; thus, the specific role of lncRNAs in post-stroke microglial activation needs further investigation. Our previous microarray analysis revealed that lncRNA U90926 was significantly induced in microglia in inflammatory status,[23] while the role of U90926 in post-stroke microglial activation has not been investigated. In this study, we aimed to investigate the role of U90926 in post-stroke microglial activation and in the pathogenesis of ischemic stroke, thus to reveal whether U90926 could be envisioned as a potential biomarker and therapeutic target for ischemic stroke.

RESULTS

U90926 is induced in microglia after experimental stroke

Since U90926 was significantly upregulated in LPS-activated microglia,[23] we first examined the level of U90926 in ischemic brain tissue and found that U90926 was significantly elevated in the penumbra of ischemic brain after 24 h of reperfusion and returned to its baseline after the third day (Figure 1A). Interestingly, the level of U90926 in the serum of transient middle cerebral artery occlusion (tMCAO) mice showed a similar expression pattern (Figure 1B). In addition to the brain, the expression levels of U90926 in other organs were also detected. U90926 was most highly expressed in the brain compared with other tissues, such as the heart, liver, kidney, and lung (Figure 1C). To further explore the expression of U90926 in post-stroke microglia *in vivo* specifically, we isolated microglia ($CD45^{int}CD11b^{+}$) from the infarct hemisphere and found that U90926 was markedly increased in post-stroke microglia, especially at the first day, which was consistent with the expression pattern of U90926 in the ischemic brain and serum of tMCAO mice (Figure 1D). Furthermore, the U90926 level in neural cells (neuron, microglia, and astrocyte) exposed to oxygen and glucose deprivation-reperfusion (OGD-R) treatment was detected via quantitative real-time PCR, and our results demonstrated that U90926 was most significantly upregulated in microglia (Figure S1). Consistently, fluorescence *in situ* hybridization (FISH) assay showed that U90926 was significantly induced in microglia and was mainly distributed in the cytoplasm after OGD-R treatment (Figure 1E). Collectively, our results revealed

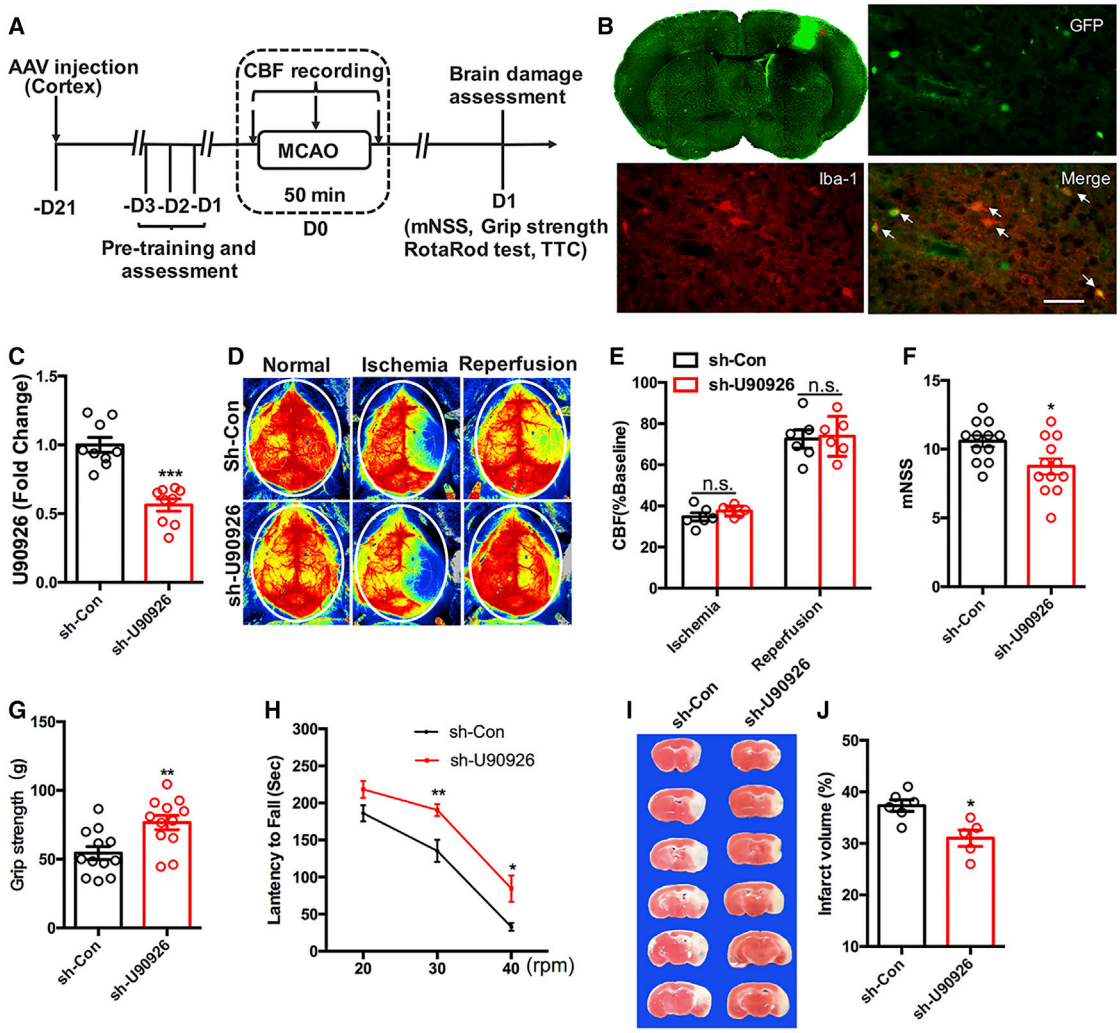

Figure 2. Microglial U90926 silencing alleviates ischemic brain injury

(A) Flowchart illustrated AAV microinjection and experimental design. (B) Distribution of U90926 shRNA-GFP AAV in the cortex 3 weeks after microinjection. Green: U90926 shRNA AAV-infected GFP-positive cells. Red: the microglia marker Iba-1. Blue: nuclei stained with DAPI. Scale bar: 25 μm. (C) The knockdown efficiency of the U90926 shRNA-GFP AAV was determined through detecting the U90926 level in microglia isolated from the ischemic hemisphere via quantitative real-time PCR. n = 9 mice per group. ***p < 0.001, unpaired Student's t test. (D and E) Regional cerebral blood flow (CBF) of the control and U90926 silencing group of mice was detected. n = 6 mice per group. n.s., no significance (p > 0.05), unpaired Student's t test. (F–H). Three weeks after AAV microinjection, tMCAO was induced. mNSS (F), grip strength (G), and the rotarod test (H) were applied to evaluate the functional outcomes of both groups of tMCAO mice. n = 12 mice per group. *p < 0.05, **p < 0.01, unpaired Student's t test. (I and J) TTC staining (I) was applied to determine the infarct volume and quantified (J). n = 6 mice in the sh-Con group and n = 5 mice in the sh-U90926 group. *p < 0.05, unpaired Student's t test. Data are presented as mean ± SEM; p values are reported in Table S1.

that U90926 was significantly induced in microglia after experimental stroke.

Microglial U90926 knockdown alleviates ischemic brain injury in tMCAO mice

To further investigate the role of microglial U90926 in the pathogenesis of ischemic stroke, mice were microinjected with the microglia-specific U90926 short hairpin RNA (shRNA)-GFP adenovirus-associated virus (AAV) (AAV-F4/80-shRNA-U90926) or control shRNA-GFP AAV (AAV-F4/80-shRNA-Con) into the right cortex (Figure 2A). The transfection efficiency of the GFP-tagged AAV was determined, and GFP was mainly detected in microglia in the cortex of mice (Figure 2B). In addition, the mRNA level of U90926 was significantly reduced in microglia isolated from the infarct hemisphere of the AAV-F4/80-shRNA-U90926-injected mice (Figure 2C). The regional cerebral blood flow (CBF) was not altered during the stroke course after microglial U90926 knockdown (Figures 2D and 2E). To explore the effect of microglial U90926 on ischemic brain injury, the neurological function was assessed. Compared with the control group, microglial U90926 silencing was found to improve

the behavioral performance of tMCAO mice, as indicated by a relatively lower modified neurological severity score (mNSS) (Figure 2F), an enhanced grip strength (Figure 2G), and an increased latency to drop from the rod in the rotarod test (Figure 2H). In addition, mice in the microglial U90926 silencing group showed reduced lesion size compared with the control group via 2,3,5-triphe-nyltetrazolium chloride (TTC) staining (Figures 2I and 2J). To summarize, these results revealed that microglia-selective U90926 knockdown mitigated ischemic brain injury in tMCAO mice.

Microglial U90926 facilitates neutrophil infiltration in experimental stroke

Next, we explored the impact of U90926 on microglial biological functions, including inflammatory phenotype, migration, phagocytosis, and chemotaxis.[1,23] To explore the effects of U90926 on microglial functions in *vitro*, the shRNA-U90926 lentivirus was used to knock down U90926 (Figure S2A). The cell viability of microglia challenged with OGD-R was found to remain unchanged after U90926 knockdown via CCK-8 assay (Figure S2B). In addition, flow cytometry analysis illustrated that U90926 inhibition did not change the pro- (CD86) or anti- (CD206) inflammatory phenotype of microglia exposed to hypoxia (Figures S2C and S2D). Consistently, the production of inflammatory cytokines was also found to remain unchanged after U90926 silencing via quantitative real-time PCR (Figure S2E). Then, the migration ability of microglia was detected via scratch tests, and we found that U90926 did not affect the migration ability of microglia exposed to hypoxia (Figures S2F and S2G). To examine the effects of U90926 on phagocytic ability of microglia, 5 μm red fluorescence microspheres (10^7/mL) were added to the medium of microglia after OGD-R treatment and detected 1 h later via flow cytometry, and our results demonstrated that the microglial phagocytosis was not significantly altered after U90926 knockdown (Figures S2H and S2I). These data suggested that U90926 did not affect the cell viability, inflammatory phenotype, migration, and phagocytosis of microglia exposed to hypoxia.

To further explore the effects of U90926 on microglial chemotaxis, the accumulation of immune cells, including microglia, B cells, $CD4^+$/$CD8^+$ T cells, and neutrophils, in ischemic brain were assessed via flow cytometry. The numbers of microglia, B cells, and $CD4^+$/$CD8^+$ T cells in the ischemic hemisphere of tMCAO mice were comparable between the control group and the microglial U90926 silencing group, while mice with microglial U90926 silencing showed a significant reduction of neutrophil infiltration (Figures 3A and 3B). Immunofluorescence staining further validated that microglial U90926 silencing induced a significant decrease of $Ly6G^+$ cells in the peri-infarct area (Figures 3C and 3D). Furthermore, quantitative real-time PCR was performed to assess the neutrophil-related inflammatory cytokines in the ischemic hemisphere, and mice with microglial U90926 knockdown showed significantly reduced neutrophil-related inflammatory cytokines, including MPO and MMP3 (Figure 3E). To assess the effects of microglial U90926 on neutrophil recruitment in experimental stroke *in vitro*, we constructed an *in vitro* model of trans-endothelial neutrophil migration (Figure 3F). More than 90% of the cells obtained using our neutrophil isolation protocol were proven to be neutrophils, which were identified by Ly6G labeling using flow cytometry (Figure S3). Fluorescein isothiocyanate (FITC)-labeled dextran leakage and trans-endothelial electrical resistance (TEER) in the Transwell system remained unchanged upon microglial U90926 silencing, indicating that microglial U90926 did not affect the BBB integrity (Figures 3G and 3H). However, it was demonstrated that fewer neutrophils transmigrated into the lower chamber after U90926 knockdown, which was consistent with the *in vivo* results (Figure 3I). Altogether, our results showed that U90926 silencing blocked microglia-induced neutrophil recruitment in experimental stroke, which might partly account for the microglial U90926-silencing-induced protective effects.

Microglial U90926 silencing fails to exert extra protective effects in neutrophil-depleted tMCAO mice

To further address our hypothesis that microglial U90926 aggravated ischemic brain injury via promoting neutrophil infiltration, the mice were intraperitoneally injected with anti-Ly6G antibodies (125 μg per mouse) 24 h before tMCAO to deplete neutrophils (Figure 4A). The depletion efficiency was validated via flow cytometry, and neutrophil proportion in the blood of mice was significantly reduced after administration of anti-Ly6G antibody (Figure 4B). Compared with the control group, the ischemic brain injury was significantly alleviated in the neutrophil-depleted mice, with reduced infarct size (Figures 4C and 4D), lower mNSS (Figure 4E), and enhanced grip strength (Figure 4F). However, microglial U90926 knockdown failed to exert extra protective effects in neutrophil-depleted tMCAO mice (Figures 4C–4F). Overall, these results demonstrated that neutrophil was a key factor that mediated the detrimental effects of microglial U90926 in ischemic stroke.

U90926 silencing decreases neutrophil chemoattractant C-X-C motif ligands

To identify the potential chemokines involved in microglial U90926-induced infiltration of neutrophils, we performed a mRNA microarray to identify the differentially expressed mRNAs in LPS-stimulated microglia with or without U90926 knockdown. As shown in the volcano and scatterplots, CXCLs, including CXCL1, CXCL2, and CXCL10, were found to be downregulated in the activated microglia with U90926 silencing (Figures 5A and 5B). We also detected the mRNA levels of the three CXCLs in the ischemic hemisphere after microglial U90926 silencing via quantitative real-time PCR and found that CXCL1 and CXCL2 were reduced after U90926 silencing and that CXCL2 was the most significantly downregulated (Figure 5C). The *in vitro* results also showed that U90926 silencing reduced the CXCL2 mRNA level in microglia exposed to hypoxia (Figure 5D). In addition, CXCL2 mRNA level in the penumbra of ischemic brain was significantly upregulated at 24 h after ischemia and displayed a similar expression pattern as U90926 (Figure 5E). Overall, our finding demonstrated that CXCL2 might contribute to microglial U90926-induced neutrophil infiltration in experimental stroke.

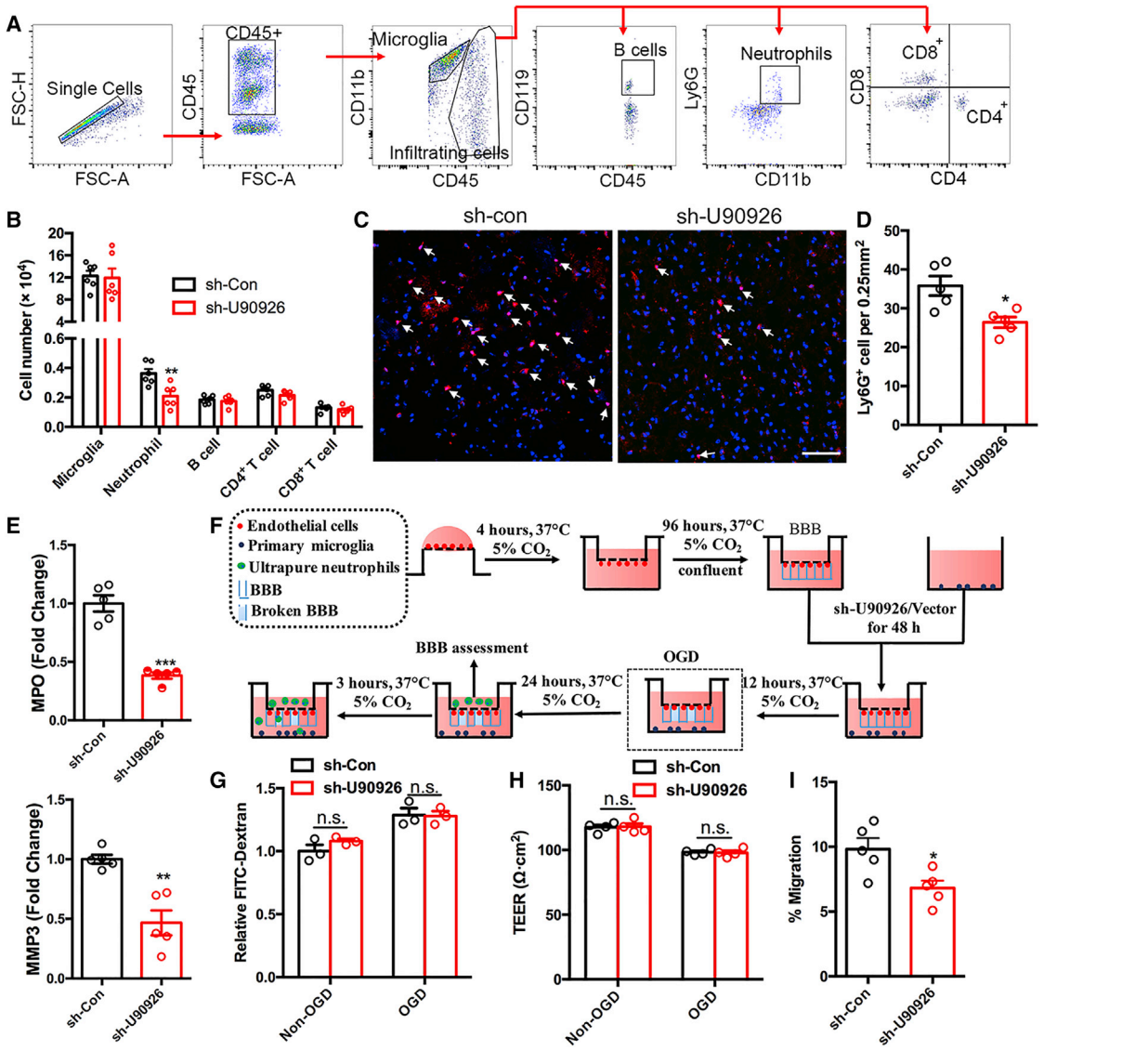

Figure 3. Microglial U90926 silencing reduces neutrophil infiltration

(A) Gating strategy for resident microglia and infiltrating immune cells isolated from the brain after tMCAO. (B) Counts of microglia, B cells, $CD4^+$ T cells, $CD8^+$ T cells, and neutrophils in brains of the control and U90926 silencing group of tMCAO mice. n = 6 mice per group, $^{**}p < 0.01$, unpaired Student's t test. (C and D) Immunofluorescence staining of neutrophils in the peri-infarct areas of the control and U90926 silencing group of tMCAO mice (C) and quantified (D). Scale bar: 50 μm. n = 5 mice per group, $^{*}p < 0.05$, unpaired Student's t test. (E) The level of neutrophil-related inflammatory cytokines, including MPO and MMP3, was detected via quantitative real-time PCR. n = 5 mice per group. $^{**}p < 0.01$, $^{***}p < 0.001$, unpaired Student's t test. (F) An *in vitro* constructed model of trans-endothelial neutrophil migration. (G) Dextran leakage was detected by a microplate reader, with the dextran leakage in the sh-Con group without OGD-R treatment normalized to 1. n = 3 per group. n.s., no significance ($p > 0.05$), unpaired Student's t test. (H) Mean TEER values were measured using a voltohmmeter. n = 4 per group. n.s., no significance ($p > 0.05$), unpaired Student's t test. (I) Neutrophil migration was measured by FCM. n = 5 per group. $^{*}p < 0.05$, unpaired Student's t test. Data are presented as mean ± SEM; p values are reported in Table S1.

U90926 protects CXCL2 mRNA from MDH2-mediated degradation

Since U90926 was mainly distributed in cytoplasm, we speculated that U90926 might induce CXCL2 expression by increasing the CXCL2 mRNA stability. The decay rate of CXCL2 mRNA was considerably increased in LPS-activated BV2 cells treated with actinomycin D (ActD) after U90926 silencing, indicating that U90926 promoted the stabilization of CXCL2 mRNA (Figure 6A). To identify the protein-binding partners of U90926, RNA pull-down followed by liquid chromatography-tandem mass spectrometry (LC-MS/MS) was performed. As shown in Figures 6B and 6C, MDH2, an identified RNA binding protein promoting the degradation of sodium channel protein

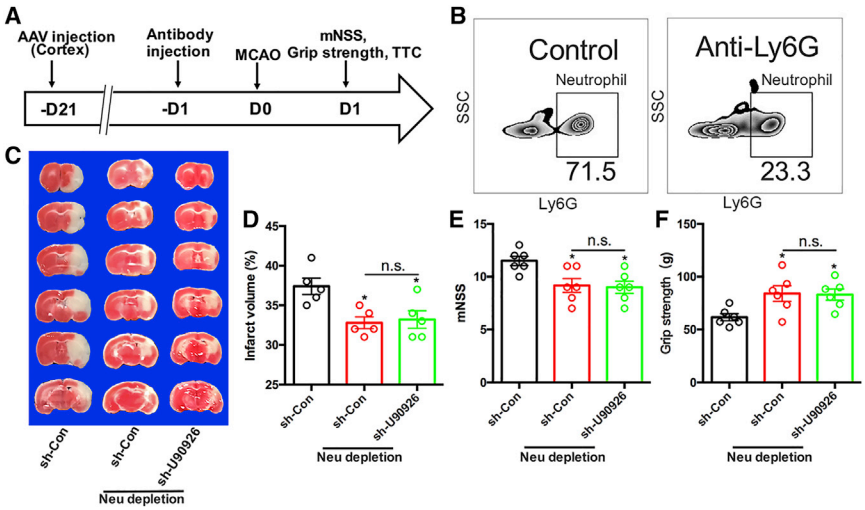

Figure 4. U90926 silencing exerts no extra protection effects on the neutrophil-depleted tMCAO mice

(A) Flowchart illustrated neutrophil depletion and experimental design. (B) Percentage of neutrophils in total white blood cells (WBCs) in the control and anti-Ly6G-antibody-administered tMCAO mice was determined by flow cytometry. (C and D) TTC staining (C) was applied to determine the infarct volume and quantified (D). n = 6 mice per group. *p < 0.05. n.s., no significance (p > 0.05), one-way ANOVA with Bonferroni post hoc test. (E and F) mNSS (E) and grip strength (F) were applied to evaluate the functional outcomes of the three groups of tMCAO mice. n = 6 mice per group. *p < 0.05. n.s., no significance (p > 0.05), one-way ANOVA with Bonferroni post hoc test. Data are presented as mean ± SEM; p values are reported in Table S1.

type 1 subunit alpha (SCN1A) mRNA in seizures,[24] was pulled down in the LPS-treated BV2 cells. RNA-binding protein immunoprecipitation (RIP) assay validated the direct binding of U90926 to MDH2 in LPS-activated BV2 cells (Figure 6D). In addition, RNA pull-down assay revealed that LPS stimulation significantly enhanced the binding of U90926 to MDH2 in primary microglia (Figure 6E), which was confirmed by FISH and immunofluorescence staining (Figure 6F).

Given the interaction between U90926 and MDH2, we hypothesized that U90926 might enhance the stability of CXCL2 mRNA via sequestering MDH2, thereby inhibiting its binding to and degrading of CXCL2 transcripts. First, we examined the effect of MDH2 on CXCL2 expression. MDH2 overexpression induced a significant reduction of CXCL2 mRNA levels in LPS-treated BV2 cells (Figure 6G), and the decay rate of CXCL2 mRNA was markedly accelerated in MDH2-overexpressing BV2 cells (Figure 6H), indicating that MDH2 could destabilize CXCL2 mRNA. We further tested whether U90926 interfered with the binding of MDH2 to CXCL2 mRNA. Interestingly, U90926 was found to reduce the direct binding between MDH2 and CXCL2 mRNA, as the enrichment of CXCL2 mRNA in the MDH2-bound RNA was significantly increased after U90926 silencing (Figure 6I). RNA binding proteins were reported to directly bind to the 3′ UTR of their downstream transcripts.[25] Here, we tested whether MDH2 might bind to the CXCL2 3′ UTR and promote its degradation. Luciferase reporter assay demonstrated that U90926 overexpression could rescue the reduction of relative luciferase activity of CXCL2 3′ UTR induced by MDH2 overexpression (Figure 6J). To further determine whether the effect of U90926 on CXCL2 was MDH2 dependent, BV2 cells with MDH2 knockdown were generated, and our results demonstrated that MDH2 knockdown induced a significant increase of CXCL2 in LPS-activated BV2 cells. In addition, U90926 silencing reversed the upregulation of CXCL2 induced by LPS stimulation, while U90926 silencing exerted no extra effects on the CXCL2 level in MDH2 knockdown BV2 cells, indicating that the modulation of CXCL2 by U90926 was MDH2 dependent (Figure 6K). Overall, our results indicated that U90926 disrupted the binding between MDH2 and CXCL2 mRNA via interacting with MDH2, thus protecting CXCL2 mRNA from MDH2-mediated degradation.

DISCUSSION

In the present study, we showed that U90926 was induced in post-stroke microglia, and microglial U90926 aggravated ischemic brain injury via facilitating neutrophil infiltration. Mechanistically, we found that U90926 directly bound to MDH2 and interfered with the binding between MDH2 and CXCL2 mRNA, thus protecting CXCL2 mRNA from MDH2-mediated degradation (Figure 7). Thus, our work indicated that U90926 might serve as a potential biomarker and therapeutic target for ischemic stroke.

Stroke triggers a robust inflammatory response, which is integral to the whole process of stroke pathogenesis and serves as a prime target for the development of new stroke therapies.[26,27] Microglia, the most important CNS resident immune cell type, are immediately activated to release inflammatory cytokines and chemokines, which aggravates the outcome of stroke.[28] Therefore, exploring the mechanisms underlying post-stroke microglial activation might provide an avenue for finding attractive therapeutic targets for stroke. Increasing evidence has demonstrated that lncRNAs participate in the modulation of microglial activation in ischemic stroke.[22,29] Our previous study demonstrated that lncRNA-1810034E14Rik reduces post-stroke microglial activation.[23] However, when conducting *in vivo* studies, bulk tissue was used in most previous studies, which might not precisely represent the characteristics of microglia. In this study, we found that lncRNA-U90926 was most significantly increased in microglia compared with other neural cells (neurons and astrocytes) when exposed to hypoxia *in vitro*. In addition, microglia were isolated from tMCAO mice using fluorescence-activated cell sorting (FACS) to specifically investigate the expression pattern of U90926 in post-stroke microglia *in vivo*. Our data demonstrated that U90926 was

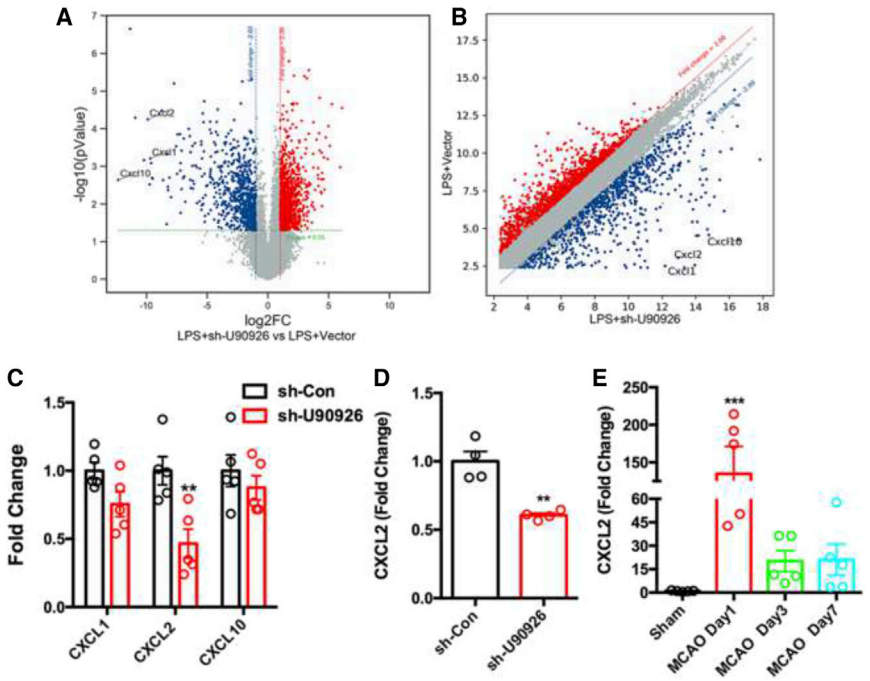

Figure 5. U90926 silencing decreases neutrophil chemoattractant C-X-C motif ligands

(A) Volcano plots displaying variations in mRNA expression in LPS-stimulated primary microglia between the control and U90926 silencing group. n = 3 per group. (B) A scatterplot assessing the significance of the differentially expressed mRNAs. n = 3 per group. (C) CXCL mRNA levels in the cortex of tMCAO mice both in the control and U90926 silencing group were detected via quantitative real-time PCR. n = 5 mice per group. **p < 0.01, unpaired Student's t test. (D) CXCL2 expression level in primary microglia exposed to OGD-R treatment was detected via quantitative real-time PCR both in the control and U90926 silencing group and quantified normalized to β-actin. n = 4 per group. **p < 0.01, unpaired Student's t test. (E) CXCL2 expression level in the tMCAO mice at various time points was detected via quantitative real-time PCR. n = 5 mice per group. ***p < 0.001 versus the sham group, one-way ANOVA with Bonferroni post hoc test. Data are presented as mean ± SEM; p values are reported in Table S1.

significantly increased in microglia in the ischemic hemispheres of tMCAO mice. Furthermore, the effect of microglial U90926 on the outcome of ischemic stroke was explored using the microglia-specific U90926 shRNA-GFP AAV (AAV-F4/80-shRNA-U90926). Our results demonstrated that microglial U90926 silencing could alleviate neurobehavioral deficits and reduce infarct size in tMCAO mice, indicating that U90926 might be a potential target for modulation of microglial activation and ischemic stroke treatment.

In addition to the microglia-associated neuroinflammation, leukocytes infiltrating into the ischemic brain following microglial activation initiate a robust inflammation response,[30,31] which further aggravates the acute ischemic injury. Among the recruited leukocytes, neutrophil infiltration is proven to aggravate ischemic brain injury in both mice and patients, as infiltrating neutrophils induced increased infarction size and BBB disruption and increased neurological scores in the acute phase of ischemic stroke.[32,33] Interestingly, the infiltration and accumulation of neutrophils in the ischemic lesion is credibly affected by microglial activities, which might further facilitate microglia to be a prime therapeutic target for stroke.[32] Otxoa-de-Amezaga et al.[34] reported that reactive microglia engulfed neutrophils at the periphery of the ischemic lesion, whereas local microglial cell loss and dystrophy occurring in the ischemic core were associated with the accumulation of neutrophils. Similarly, Neumann et al.[35] reported that brain-resident microglia formed cytoplasmic processes to trap infiltrating neutrophils. However, in addition to trapping and engulfing neutrophils, microglia directly participated in the recruitment of neutrophils. Li et al.[2] reported that upregulation of ZEB1 in microglia inhibited the production of astrocytic CXCL1 and thus led to a decline of neutrophil infiltration into the brain in experimental stroke. However, the specific interaction between microglia and neutrophils and the underlying mechanisms in ischemic stroke remain poorly understood. In our study, using flow cytometry and immunofluorescence staining assays, we found that microglial U90926 silencing significantly inhibited the recruitment of neutrophils into the ischemic brain of tMCAO mice, which was further validated using an *in vitro* model of trans-endothelial neutrophil migration. Moreover, we found that microglial U90926 silencing failed to exert extra protective effects in neutrophil-depleted tMCAO mice, which further validated our finding that U90926 aggravated ischemic brain injury via promoting neutrophil infiltration in experimental stroke. Overall, we illustrated that microglia could directly affect the recruitment of neutrophils. In detail, we revealed that microglial U90926 facilitated microglia-induced neutrophil infiltration, indicating that U90926 might be a potential target for modulating post-stroke neuroinflammation.

U90926 was first reported by a genome exploration research group as a lncRNA.[36] Chen et al.[37] reported that U90926 was predominantly expressed in adipose in normal mice and attenuated 3T3-L1 adipocyte differentiation via inhibiting peroxisome proliferator-activated receptor γ2 (PPARγ2) or PPARγ. Interestingly, our study demonstrated that U90926 was mainly clustered in microglia in stroke mice and facilitated neutrophil infiltration. Recent studies revealed that lncRNA could bind to RNA-binding protein (RBP) and protect RBP-mediated degradation of their target genes.[25,38] Here, we found that U90926 directly bound to MDH2, a metabolic enzyme, to participate in the citric acid cycle via catalyzing the conversion of malate to oxaloacetate.[39] Mutations in MDH2 cause early-onset encephalopathy,[39] and MDH2 was also reported to act as an identified RNA-binding protein facilitating the degradation of SCN1A mRNA via binding to the conserved

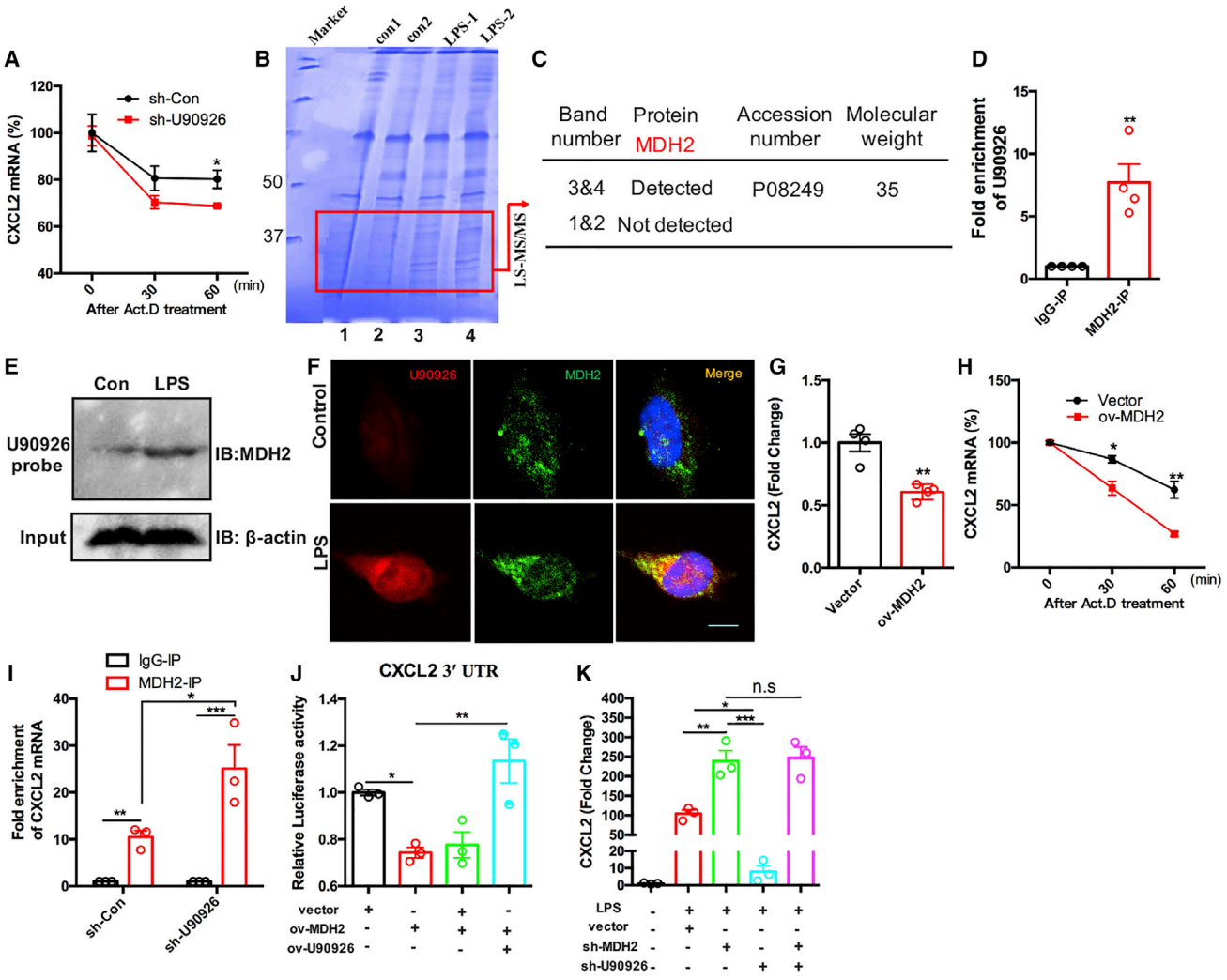

Figure 6. U90926 protects CXCL2 mRNA from MDH2-mediated degradation

(A) The mRNA level of CXCL2 in LPS-stimulated BV2 cells was detected by quantitative real-time PCR after 30 min and 60 min treatment with ActD both in the control group and U90926 silencing group. The relative CXCL2 mRNA level (CXCL2/β-actin) in the BV2 cells before treatment was normalized as 100%. n = 3 per group. *$p < 0.05$, unpaired Student's t test. (B and C) BV2 cell were treated with LPS (100 ng/mL) for 3 h, the whole lysates were mixed with U90926 probe (containing biotin) binding protein beads, and the eluted protein was subjected to SDS/PAGE. (B) The gel of the complex was stained by Coomassie brilliant blue (CBB) after SDS/PAGE, and the different expressed compartment was analyzed by LC-MS/MS. MDH2 was identified in the RBPs pulled down using U90926-specific probe in the LPS-stimulated BV2 cells (C). (D) MDH2 protein in BV2 cells treated with LPS for 3 h was immunoprecipitated with anti-MDH2-coated protein A/G magnetic beads, and the MDH2-bound U90926 level was analyzed via quantitative real-time PCR. n = 4 per group. **$p < 0.01$, unpaired Student's t test. (E) Biotin-labeled U90926 probe was incubated with lysates of LPS-stimulated BV2 cells, and the MDH2 protein was detected by immunoblot analysis. (F) Co-localization of U90926 and MDH2 detected by FISH and immunofluorescence staining, respectively. Scale bar: 10 μm. (G) CXCL2 mRNA level in the LPS-stimulated BV2 cells was detected via quantitative real-time PCR both in the control and MDH2-overexpression groups and quantified normalized to β-actin. n = 4 per group. **$p < 0.01$, unpaired Student's t test. (H) The CXCL2 mRNA stability in BV2 cells both in the control and MDH2-overexpression group was detected as (A) demonstrated. n = 3 per group. *$p < 0.05$, **$p < 0.01$, unpaired Student's t test. (I). MDH2 protein-bound CXCL2 mRNA level both in the control and U90926 silencing group was detected via quantitative real-time PCR. n = 3 per group. *$p < 0.05$, **$p < 0.01$, ***$p < 0.001$, unpaired Student's t test. (J) HEK293T cells were transfected with U90926/MDH2 plasmid, and 24 h later the cells were transfected with the pGL3-luciferase vector encoding the full length of CXCL2 3′ UTR. The relative luciferase activity was determined at 48 h post transfection. n = 3 per group. *$p < 0.05$, **$p < 0.01$, one-way ANOVA with Bonferroni post hoc test. (K) CXCL2 mRNA in BV2 cells with various kinds of treatments was detected with quantitative real-time PCR and quantified normalized to β-actin. n = 3 per group. *$p < 0.05$, **$p < 0.01$, ***$p < 0.001$, one-way ANOVA with Bonferroni post hoc test. Data are presented as mean ± SEM; p values are reported in Table S1.

regions of 3′ UTR under seizure conditions.[24] Interestingly, our results demonstrated that MDH2 bound to CXCL2 mRNA and promoted its degradation, while the binding between U90926 and MDH2 blocked the binding of MDH2 to CXCL2 mRNA, thus inducing an upregulation of CXCL2 following ischemic stroke. CXCL2 was a kind of widely studied chemokine with strong neutrophil chemoattractant activity via

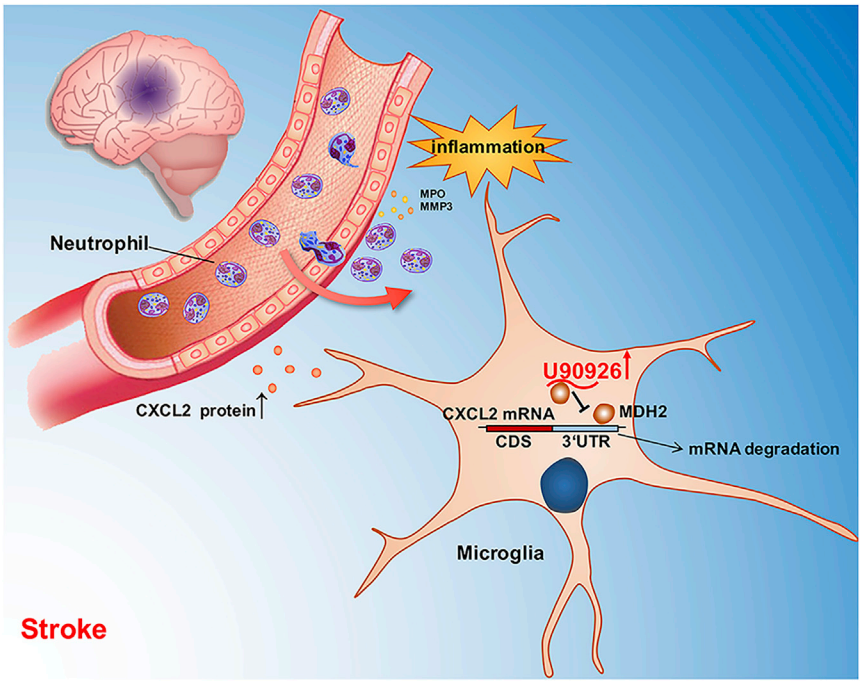

Figure 7. Schematic diagram of the proposed mechanisms underlying the role of microglial lnc-U90926 in ischemic stroke

CXCR2,[40] which we found in this study might be a key mediator underlying the action of microglial U90926 in facilitating neutrophil infiltration in ischemic stroke. However, CXCL2 is also produced by several kinds of other immune cells;[41] whether U90926 modulates the production of CXLC2 of those cells needs our further exploration. In addition, the binding domain or surface structure of U90926 and MDH2 also merits our further investigation.

In summary, we showed that lnc-U90926 was significantly induced in microglia in ischemic stroke, and microglial U90926 silencing could alleviate ischemic brain injury. Furthermore, microglial U90926 directly bound to MDH2 and competitively reduced the MDH2-mediated degradation of CXCL2 mRNA, thus promoting the infiltration of neutrophils. Collectively, our study demonstrated that U90926 might be a potential biomarker and therapeutic target for ischemic stroke.

MATERIALS AND METHODS

Animals

Male C57BL/6J (B6) mice were purchased from the Model Animal Research Center of Nanjing University. All animal experiments were performed under the guidelines of the Animal Use and Care Committees at Nanjing University. All efforts were spared to alleviate the suffering of mice.

tMCAO

Unilateral focal cerebral ischemia was induced in 8-week-old mice by tMCAO using the intraluminal filament technique as previously described.[42] Briefly, after being anesthetized, a midline neck incision was made under a dissecting microscope. Then, the right common carotid artery (CCA) and external carotid artery (ECA) were isolated. A 12-mm-long 6-0 silicon-coated monofilament suture was introduced into a wedge-shaped incision on the ECA and further inserted to the circle of Willis to achieve the middle cerebral artery occlusion. After 50 min of occlusion, the filament was withdrawn to achieve reperfusion. Mice were included if the Doppler laser reading was reduced more than 20% of baseline. Animals that died or failed to display a CBF reduction of 20% of the baseline were excluded from further study. Sham-treated mice were subjected to the same procedure without tMCAO. Mice both in the sham and tMCAO groups were kept in an air-conditioned room at 21°C ± 1°C with a 12 h light/dark cycle. A final tally of 175 mice (18 sham-operated and 157 ischemic mice) were used in this study, including 21 mice that were excluded from further assessments either because of death (15) after ischemia or failure of ischemia induction (6). No animals died from the sham procedure.

Primary microglial culture

Primary microglial cells were isolated and purified from 1-day-old C57BL/6J mice as described previously.[5] In brief, the cerebral cortex of the mice was digested, followed by centrifuging and filtering to get the glial cells. Then the cells obtained were seeded into 75 cm^2 flasks and cultured for 14 days. Microglial cells were acquired by gently shaking the flasks and were re-plated onto indicated plates.

OGD-R

OGD-R was performed as described previously.[42] In brief, the cells were cultured in deoxygenated DMEM (Invitrogen, Carlsbad, CA, USA) without glucose and fetal bovine serum (FBS, Invitrogen, Carlsbad, CA, USA). Then, the plates were transferred into an incubator with premixed gas (5% CO_2 and 95% N_2 without oxygen) for 4 h at 37°C, and the cells were subjected to normal medium in normal incubator for 12–24 h to achieve reperfusion. Non-OGD samples were cultured in sister plates exposed to the same treatment with the exception of the oxygen and glucose deprivation.

RNA isolation and quantitative real-time PCR

Total RNA of the cells and tissues was extracted using a TRIzol commercial kit (Invitrogen, Carlsbad, CA, USA) according to the standard protocol, and RNA in the serum of mice was extracted with a miRNeasy Serum/Plasma Kit (QIAGEN, Hilden, Germany). Then, RNA was reverse-transcribed into cDNA with a PrimeScript RT

Table 1. Primers sequence

U90926	forward	5′-TTCTCTGACTGGGGGTCCTC-3′
	reverse	5′-AGCTGGAAGCATGATCCGAC-3′
CXCL1	forward	5′-TGCACCCAAACCGAAGTCAT-3′
	reverse	5′-CTCCGTTACTTGGGGACACC-3′
CXCL2	forward	5′-CCAACCACCAGGCTACAGG-3′
	reverse	5′-GCGTCACACTCAAGCTCTG-3′
CXCL10	forward	5′-CCAAGTGCTGCCGTCATTTTC-3′
	reverse	5′-GGCTCGCAGGGATGATTTCAA-3′
GAPDH	forward	5′-GCCAAGGCTGTGGGCAAGGT-3′
	reverse	5′-TCTCCAGGCGGCACGTCAGA-3′
β-actin	forward	5′-TGAGCTGCGTTTTACACCCT-3′
	reverse	5′-TTTGGGGGATGTTTGCTCCA-3′

reagent Kit (Vazyme Biotech, Nanjing, China). Quantitative real-time PCR was implemented on an ABI 7500 PCR instrument (Applied Biosystems, Carlsbad, CA, USA) with a SYBR green kit (Takara, Carlsbad, CA, USA). Relative mRNA expression level was quantified normalized to GAPDH or β-actin, and those quantified normalized to β-actin were mentioned in the corresponding figure legends. The sequences of primers used are listed in Table 1.

Microarray processing

The Agilent SurePrint G3 Mouse GE V2.0 microarray was performed by oebiotech of Shanghai, China. Briefly, total RNA from primary microglia was transcribed to double-strand cDNA after being purified using RNeasy Mini Kit (QIAGEN, Hilden, German). Then, the cDNA was synthesized into cRNA to be hybridized onto the microarray. The array images were scanned with Agilent Scanner G2505C (Agilent Technologies, Shanghai, China). Differentially expressed genes were picked out with the fold change $\geq$ 2.0 and adjusted p value <0.05.

FISH

FISH assay was performed according to the previous study.[43] Briefly, cells were fixed in 4% formaldehyde and then permeabilized in PBS containing 0.5% Triton X-100. Hybridization was carried out using a FISH kit (RiboBio, Gaungzhou, China) according to the manufacturer's instructions. Hybridization buffer containing 50 nM of a commercially available U90926-specific probe was added to the cells and incubated at 37°C overnight. The next day, cells were rinsed thrice with 4× SSC solution (20× SSC solution: 175.3 g NaCl and 88.2 g sodium citrate diluted in ultra-pure water, with the volume adjusted to 1 L and pH adjusted to 7.0) with 0.1% Tween-20 for 5 min at 42°C, followed by washing once with 2× SSC solution and once with 1× SSC solution for 5 min each at 42°C. After being stained with 4′,6-diamidino-2-phenylindole (DAPI), images were obtained using a confocal microscope (Olympus X73, Fukasawa, Japan).

Microinjection of AAV

Mice were fixed in a stereotactic frame after being anesthetized. Then, mice were microinjected with either the microglia-specific control shRNA-GFP AAV (AAV-F4/80-shRNA-Con) or U90926 shRNA-GFP AAV (AAV-F4/80-shRNA-U90926) (1 μL of 1×10^{12} viral genomes/μL, Genechem Techniques, Shanghai, China) into the right cortex at the following three microinjection coordinates: anteroposterior, −0.3/0.8/1.9 mm; lateral, 3.0 mm; and ventral, −1.8 mm. The sequence for shU90926 was: shU90926: 5′-CCACTGAGCAGAAGAACTA-3′, the control sequence was: 5′-TTCTCCGAACGTGTCACGT-3′.

Cortical CBF measurements

CBF was measured in the tMCAO mice using a two-dimensional laser speckle imaging system (Moor Instruments, UK) or laser doppler flowmetry as previously described.[44] Mice were subjected to repeated CBF measurements at three time points: 15 min before MCAO, during MCAO, and 15 min after the initiation of reperfusion. CBF changes were displayed as a percentage of pre-tMCAO baseline.

Neurobehavioral examination

Neurological performance of the tMCAO mice was evaluated using the mNSS, rotarod test, and grip strength assays as described previously.[5] The mNSS was determined using a scale graded between 0 and 18, with 0 corresponding to a normal score and 18 corresponding to a maximal deficit score to assess the motor, sensory, reflex, and balance deficits of mice. Mice were placed on a rotarod rod (Nature Gene Corporation, Beijing, China) rotating at different speeds. The time duration for each mouse holding on the rotating stick was recorded (maximum time: 300 s). Grip strength was evaluated using a Panlab machine (LE902, Bioseb, Pinellas Park, FL, USA). Neurobehavioral tests were evaluated by 2 experimenters blinded to our study.

Infarct volume measurement

Infarct volume was measured at 24 h after tMCAO using 0.2% (w/v) TTC (Sigma-Aldrich, St. Louis, MO, USA). Briefly, mice were euthanized and decapitated, and the brains were collected and immediately frozen at −20°C for 5 min. Then the brains were cut into 6 1-mm slices and incubated with TTC solution for 10–30 min and then fixed in 4% paraformaldehyde (PFA) to determine the infarct volume (mainly including infarct cortex and striatum). The infarct area mainly included the pale gray color area representing infarct tissues and the dark red color representing normal brain tissues. Images were acquired using a digital camera and analyzed using ImageJ software. Infarct volume was calculated by integration of the infarct areas for the 6 slices of each brain and calculated as described previously.[45] Infarct size = (contralateral area − ipsilateral non-infarct area)/contralateral area × 100%.

Cell viability assessment

After being treated with lentivirus carrying sh-U90926 (MOI = 50, Genechem Techniques, Shanghai, China) for 48 h, cell counting kit-8 (CCK-8) analysis was used to measure the cell viability of primary microglia cultured in 96-well plates. In brief, 10 μL of CCK-8 solution (5 mg/mL; Sigma, St. Louis, MO, USA) was added to each well. After being incubated at 37°C for 2 h, the absorbance at 450 nm was measured using a microplate reader (Tecan, Switzerland).

Flow cytometry, microglia, and neutrophil isolation

Mice were transcardially perfused with 50 mL cold PBS containing 5 IU/mL heparin, and brains were isolated in 1× Hank's balanced salt solution (HBSS) with 25% glucose and HEPES. Single-cell suspensions were obtained from the infarcted brain of tMCAO mice using the Neural Tissue Dissociation Kit (Miltenyi Biotec, Auburn, CA, USA) according to the manufacturer's instructions. The total mixture obtained was passed through a 70 μm pore filter and then stratified on a 30%–70% Percoll gradient (GE Healthcare BioSciences, Piscataway, NJ, USA). After centrifuging at 2,500 rpm for 20 min, cells at the interface were collected and stained with fluorophore-labeled anti-mouse CD45 (Invitrogen, 25-0451-82, 1:200), CD11b (Invitrogen, 53-0112-82, 1:200), Ly6G (Invitrogen, 12-9668-82, 1:200), CD19 (Invitrogen, 17-0193-82, 1:200), CD4 (Invitrogen, 12-0041-82, 1:200), and CD8 (Invitrogen, 17-0081-82, 1:200). FACS (BD Biosciences, Carlsbad, CA, USA) was used for flow cytometry analysis and to isolate microglia ($CD45^{int}CD11b^{+}$) from the ischemic brain tissue. Neutrophils were collected from the bone marrow of mice as described previously.[46] Bone marrow cells were flushed from the femora and tibia of mice and treated with ACK lysis buffer to clear red cells after centrifuging at 1,500 rpm for 5 min. After washing with PBS, cells were stained with PE-conjugated Ly6G antibody (Invitrogen, 12-9668-82, 1:200), and then the cells were labeled with magnetic anti-PE microbeads (BD Biosciences, Carlsbad, CA, USA). Finally, the cells were separated using a MACS column and MACS separator according to the manufacturer's instructions.

Immunofluorescence staining

Experimental mice were anesthetized and then perfused with PBS followed by 4% PFA to fix. The brains were quickly removed and placed in 4% PFA. After dehydrating, brains were sectioned at the thickness of 20 μm. Microglia were fixed in 4% PFA for 15 min at room temperature. Brain tissues and cells were permeabilized with 0.25% Triton X-100 for 20 min followed by blocking in blocking buffer (1× PBS containing 5% bovine serum albumin and 0.1% Triton X-100) for 90 min and then incubated with indicated primary antibodies (MDH2, Santa Cruz, sc-293474, 1:200; Iba-1, Abcam, ab48004, 1:500; Ly6G, Abcam, ab25377, 1:200) overnight at 4°C. On the second day, the brain tissues or the cells were incubated with secondary antibodies (1:500, Invitrogen, Carlsbad, CA, USA) for 2 h at room temperature in the dark. The nuclei were counterstained with DAPI (Beyotime Biotechnology, Nanjing, China) for 15 min in the dark. Images were obtained using a fluorescence microscope (Olympus X73, Fukasawa, Japan).

Neutrophil migration model

The in *vitro* neutrophil migration model was constructed as described previously with some improvements.[47] Endothelial cells (Bend3) were seed onto the underside of a Transwell. Four hours later, the Transwell was inverted and the endothelial cells were allowed to develop a confluent endothelial monolayer (BBB model) for 96 h in media. Then, the Transwell was transferred into another 12-well plate, in which primary microglia having been transfected with sh-U90926 or sh-Con lentivirus for 48 h were cultured. Twelve hours later, both the endothelial cells and microglia were exposed to OGD treatment for 4 h. Following 24 h of reperfusion, ultrapure neutrophils were added to the basolateral side of the Transwell and allowed migration for 3 h.

Measurement of TEER

To evaluate the permeability of our *in vitro* BBB model, the TEER of the Bend3 monolayer was measured after 12 h re-oxygenation following OGD, with a portable endothelial voltohmmeter (EVOM, World Precision Instruments, Sarasota, FL, USA) according to the manufacturer's instruction. All independent experiments were measured in triplicate, with a blank Transwell set as a control.

FITC-dextran transendothelial permeability assay

The FITC-dextran transendothelial permeability assay was applied to assess the integrity of the Bend3 monolayer. Briefly, after 12 h reoxygenation following OGD-R, 0.1 mg/mL of FITC-labeled dextran (MW, 70,000, Sigma-Aldrich) was added to the upper compartment. After incubation for another 20 min, 100 μL of supernatant from the lower chamber was analyzed via a microplate reader (excitation 490 nm, emission 520 nm). All independent experiments were measured in triplicate.

Neutrophil depletion

To construct neutrophil-depleted mice, *in vivo* anti-mouse Ly6G antibody (GeneTex, GTX00669, Irvine, CA, USA) was intraperitoneally injected 1 day before surgery (150 μg/mouse). The neutrophil population in the blood of mice was then monitored using FACS.

RNA stability assay

Primary microglia were stimulated with LPS (100 ng/mL) for 3 h and then treated with ActD (1 μg/mL) to inhibit the activity of RNA polymerase II. Total RNA was then obtained at indicated time points and quantified via quantitative real-time PCR.

RNA pull-down

Biotin-labeled RNA oligonucleotides (U90926: biotin-ACAGUAGUUCUUCUGCUCAGUGGCG) were synthesized by GenePharma Technologies (Shanghai, China) and mixed with streptavidin-coated magnetic beads (MCE, HY-K0208) in 100 μL binding buffer (10 mM HEPES [pH 7.6], 50 mM KCl, 1 mM EDTA, 0.05% Triton X-100, 5% glycerol, 1 mM dithiothreitol, and 40 U/mL RNasin) at 37°C for 2–3 h. Then, U90926 probe-conjugated magnetic beads were added to 300 μg cell lysates of LPS (100 ng/mL)-stimulated BV2 cells in binding buffer for 2 h at 4°C. After washing 4 times, the beads were resuspended using 1× western blot loading buffer and prepared for the following LS-MS/MS (mass spectrometry, oebiotech, Shanghai, China) and western blot analysis.

RIP

RIP was conducted according to the instructions of the Magna RIP Kit (Millipore, Boston, MA, USA). Briefly, RIP lysis buffer supplied was used to obtain RIP lysates from BV2 cells at first. Then, 5 μg of MDH2 (Santa Cruz, sc-293474) antibody or control rabbit IgG

(Cell Signaling Technology, #2729) was incubated with protein A/G magnetic beads in RIP Wash Buffer for 1 h at room temperature. After washing with RIP Wash Buffer three times, beads were added to the acquired RIP lysates in RIP Immunoprecipitation Buffer and incubated at 4°C overnight. On the second day, after washing 6 times, beads were resuspended in Proteinase K Buffer and incubated at 55°C for 30 min for protein digestion. RNA was acquired using RNA extraction buffer (phenol:chloroform:isoamyl alcohol [125:24:1]) and analyzed by quantitative real-time PCR.

RNA interference

Lentivirus carrying U90926/MDH2 shRNA was used to knockdown U90926 or MDH2, while gene-overexpression (U90926, MDH2) plasmid (GenePharma Techniques, Shanghai, China) was used to overexpress the target gene.

Dual-luciferase reporter assay

The HEK293T cells were plated at a density of 1×10^5 cells per well in a 12-well plate and transfected with empty vector or gene-overexpression (U90926, MDH2) plasmid. Twenty-four hours later, transfected HEK293T cells were further transfected with pGL3-luciferase plasmid encoding the CXCL2 3′ UTR. The firefly and Renilla luciferase activity in the lysates were determined using the Dual Luciferase Reporter Assay System (Promega, Madison, WI, USA) at 24 h, as described previously.[48] The Renilla luciferase gene was set as an internal control. All experiments were conducted with three replicates.

Statistics analysis

The data were displayed as the mean ± standard error of the mean (SEM). Statistical analysis was performed using SPSS 17.0 (SPSS, Chicago, IL, USA). The difference between two groups was analyzed using unpaired Student's t test, and the difference among multiple groups was analyzed by one-way analysis of variance (ANOVA) with repeated measures followed by Bonferroni post hoc test. A statistically significant difference was set at $p < 0.05$.

Data accessibility

The microarray data are deposited in the Gene Expression Omnibus (GEO) database with the accession number GEO: GSE159903. All other data are available from the corresponding author upon reasonable request.

SUPPLEMENTAL INFORMATION

Supplemental information can be found online at https://doi.org/10.1016/j.ymthe.2021.04.025.

ACKNOWLEDGMENTS

This work was supported by grants from the National Natural Science Foundation of China (81630028 and 81920108017 to Y.X.).

AUTHOR CONTRIBUTIONS

Y.X. designed research; J.C., J.J., X.Z., H.Y., L.Y., P.L., X.D., Y.G., X.B., and S.X. performed experiments; J.C. and J.J. analyzed data; J.C. and J.L. wrote the manuscript; X.Z., X.C., and Y.C. provided valuable comments and revised the manuscript. All authors read and approved the final version of the manuscript.

DECLARATION OF INTERESTS

The authors declare no competing interests.

REFERENCES

1. Ma, Y., Wang, J., Wang, Y., and Yang, G.Y. (2017). The biphasic function of microglia in ischemic stroke. Prog. Neurobiol. *157*, 247–272.
2. Li, D., Lang, W., Zhou, C., Wu, C., Zhang, F., Liu, Q., Yang, S., and Hao, J. (2018). Upregulation of Microglial ZEB1 Ameliorates Brain Damage after Acute Ischemic Stroke. Cell Rep. *22*, 3574–3586.
3. Zhang, M.J., Zhao, Q.C., Xia, M.X., Chen, J., Chen, Y.T., Cao, X., Liu, Y., Yuan, Z.Q., Wang, X.Y., and Xu, Y. (2020). The HDAC3 inhibitor RGFP966 ameliorated ischemic brain damage by downregulating the AIM2 inflammasome. FASEB J. *34*, 648–662.
4. Kang, L., Yu, H., Yang, X., Zhu, Y., Bai, X., Wang, R., Cao, Y., Xu, H., Luo, H., Lu, L., et al. (2020). Neutrophil extracellular traps released by neutrophils impair revascularization and vascular remodeling after stroke. Nat. Commun. *11*, 2488.
5. Meng, H., Zhao, H., Cao, X., Hao, J., Zhang, H., Liu, Y., Zhu, M.S., Fan, L., Weng, L., Qian, L., et al. (2019). Double-negative T cells remarkably promote neuroinflammation after ischemic stroke. Proc. Natl. Acad. Sci. USA *116*, 5558–5563.
6. Planas, A.M. (2018). Role of Immune Cells Migrating to the Ischemic Brain. Stroke *49*, 2261–2267.
7. Tang, C., Wang, C., Zhang, Y., Xue, L., Li, Y., Ju, C., and Zhang, C. (2019). Recognition, Intervention, and Monitoring of Neutrophils in Acute Ischemic Stroke. Nano Lett. *19*, 4470–4477.
8. García-Culebras, A., Durán-Laforet, V., Peña-Martínez, C., Ballesteros, I., Pradillo, J.M., Díaz-Guzmán, J., Lizasoain, I., and Moro, M.A. (2018). Myeloid cells as therapeutic targets in neuroinflammation after stroke: Specific roles of neutrophils and neutrophil-platelet interactions. J. Cereb. Blood Flow Metab. *38*, 2150–2164.
9. Peiseler, M., and Kubes, P. (2019). More friend than foe: the emerging role of neutrophils in tissue repair. J. Clin. Invest. *129*, 2629–2639.
10. Cserép, C., Pósfai, B., Lénárt, N., Fekete, R., László, Z.I., Lele, Z., Orsolits, B., Molnár, G., Heindl, S., Schwarcz, A.D., et al. (2020). Microglia monitor and protect neuronal function through specialized somatic purinergic junctions. Science *367*, 528–537.
11. Lan, X., Han, X., Li, Q., Yang, Q.W., and Wang, J. (2017). Modulators of microglial activation and polarization after intracerebral haemorrhage. Nat. Rev. Neurol. *13*, 420–433.
12. Zhang, C.Y., Dong, X., Gao, J., Lin, W., Liu, Z., and Wang, Z. (2019). Nanoparticle-induced neutrophil apoptosis increases survival in sepsis and alleviates neurological damage in stroke. Sci. Adv. *5*, eaax7964.
13. Koh, H.S., Chang, C.Y., Jeon, S.B., Yoon, H.J., Ahn, Y.H., Kim, H.S., Kim, I.H., Jeon, S.H., Johnson, R.S., and Park, E.J. (2015). The HIF-1/glial TIM-3 axis controls inflammation-associated brain damage under hypoxia. Nat. Commun. *6*, 6340.
14. Cai, W., Liu, S., Hu, M., Huang, F., Zhu, Q., Qiu, W., Hu, X., Colello, J., Zheng, S.G., and Lu, Z. (2020). Functional Dynamics of Neutrophils After Ischemic Stroke. Transl. Stroke Res. *11*, 108–121.
15. Drummond, R.A., Swamydas, M., Oikonomou, V., Zhai, B., Dambuza, I.M., Schaefer, B.C., Bohrer, A.C., Mayer-Barber, K.D., Lira, S.A., Iwakura, Y., et al. (2019). CARD9$^+$ microglia promote antifungal immunity via IL-1β- and CXCL1-mediated neutrophil recruitment. Nat. Immunol. *20*, 559–570.
16. Xie, Y., Guo, H., Wang, L., Xu, L., Zhang, X., Yu, L., Liu, Q., Li, Y., Zhao, N., Zhao, N., et al. (2017). Human albumin attenuates excessive innate immunity via inhibition of microglial Mincle/Syk signaling in subarachnoid hemorrhage. Brain Behav. Immun. *60*, 346–360.
17. Kim, N.D., and Luster, A.D. (2015). The role of tissue resident cells in neutrophil recruitment. Trends Immunol. *36*, 547–555.
18. Akbarpour, M., Lecuona, E., Chiu, S.F., Wu, Q., Querrey, M., Fernandez, R., Núñez-Santana, F.L., Sun, H., Ravi, S., Kurihara, C., et al. (2020). Residual endotoxin induces

primary graft dysfunction through ischemia/reperfusion-primed alveolar macrophages. J. Clin. Invest. *130*, 4456–4469.

19. Tiedt, S., and Dichgans, M. (2018). Role of Non-Coding RNAs in Stroke. Stroke *49*, 3098–3106.
20. Ponting, C.P., Oliver, P.L., and Reik, W. (2009). Evolution and functions of long noncoding RNAs. Cell *136*, 629–641.
21. Dykstra-Aiello, C., Jickling, G.C., Ander, B.P., Shroff, N., Zhan, X., Liu, D., Hull, H., Orantia, M., Stamova, B.S., and Sharp, F.R. (2016). Altered Expression of Long Noncoding RNAs in Blood After Ischemic Stroke and Proximity to Putative Stroke Risk Loci. Stroke *47*, 2896–2903.
22. Wang, J., Zhao, H., Fan, Z., Li, G., Ma, Q., Tao, Z., Wang, R., Feng, J., and Luo, Y. (2017). Long Noncoding RNA H19 Promotes Neuroinflammation in Ischemic Stroke by Driving Histone Deacetylase 1-Dependent M1 Microglial Polarization. Stroke *48*, 2211–2221.
23. Zhang, X., Zhu, X.L., Ji, B.Y., Cao, X., Yu, L.J., Zhang, Y., Bao, X.Y., Xu, Y., and Jin, J.L. (2019). LncRNA-1810034E14Rik reduces microglia activation in experimental ischemic stroke. J. Neuroinflammation *16*, 75.
24. Chen, Y.H., Liu, S.J., Gao, M.M., Zeng, T., Lin, G.W., Tan, N.N., Tang, H.L., Lu, P., Su, T., Sun, W.W., et al. (2017). MDH2 is an RNA binding protein involved in downregulation of sodium channel Scn1a expression under seizure condition. Biochim. Biophys. Acta Mol. Basis Dis. *1863*, 1492–1499.
25. Kulkarni, S., Lied, A., Kulkarni, V., Rucevic, M., Martin, M.P., Walker-Sperling, V., Anderson, S.K., Ewy, R., Singh, S., Nguyen, H., et al. (2019). CCR5AS lncRNA variation differentially regulates CCR5, influencing HIV disease outcome. Nat. Immunol. *20*, 824–834.
26. Shi, K., Tian, D.C., Li, Z.G., Ducruet, A.F., Lawton, M.T., and Shi, F.D. (2019). Global brain inflammation in stroke. Lancet Neurol. *18*, 1058–1066.
27. Liberale, L., Bonetti, N.R., Puspitasari, Y.M., Schwarz, L., Akhmedov, A., Montecucco, F., Ruschitzka, F., Beer, J.H., Lüscher, T.F., Simard, J., et al. (2020). Postischemic Administration of IL-1α Neutralizing Antibody Reduces Brain Damage and Neurological Deficit in Experimental Stroke. Circulation *142*, 187–189.
28. Tsuyama, J., Nakamura, A., Ooboshi, H., Yoshimura, A., and Shichita, T. (2018). Pivotal role of innate myeloid cells in cerebral post-ischemic sterile inflammation. Semin. Immunopathol. *40*, 523–538.
29. Deng, Y., Chen, D., Wang, L., Gao, F., Jin, B., Lv, H., Zhang, G., Sun, X., Liu, L., Mo, D., et al. (2019). Silencing of Long Noncoding RNA Nespas Aggravates Microglial Cell Death and Neuroinflammation in Ischemic Stroke. Stroke *50*, 1850–1858.
30. Drieu, A., Buendia, I., Levard, D., Hélie, P., Brodin, C., Vivien, D., and Rubio, M. (2020). Immune Responses and Anti-inflammatory Strategies in a Clinically Relevant Model of Thromboembolic Ischemic Stroke with Reperfusion. Transl. Stroke Res. *11*, 481–495.
31. Fan, L., Zhang, C.J., Zhu, L., Chen, J., Zhang, Z., Liu, P., Cao, X., Meng, H., and Xu, Y. (2020). FasL-PDPK1 Pathway Promotes the Cytotoxicity of $CD8^+$ T Cells During Ischemic Stroke. Transl. Stroke Res. *11*, 747–761.
32. Neumann, J., Sauerzweig, S., Rönicke, R., Gunzer, F., Dinkel, K., Ullrich, O., Gunzer, M., and Reymann, K.G. (2008). Microglia cells protect neurons by direct engulfment of invading neutrophil granulocytes: a new mechanism of CNS immune privilege. J. Neurosci. *28*, 5965–5975.
33. Jickling, G.C., and Dziedzic, T. (2019). Neutrophil count is related to stroke outcome following endovascular therapy. Neurology *93*, 194–195.
34. Otxoa-de-Amezaga, A., Miró-Mur, F., Pedragosa, J., Gallizioli, M., Justicia, C., Gaja-Capdevila, N., Ruíz-Jaen, F., Salas-Perdomo, A., Bosch, A., Calvo, M., et al. (2019). Microglial cell loss after ischemic stroke favors brain neutrophil accumulation. Acta Neuropathol. *137*, 321–341.
35. Neumann, J., Riek-Burchardt, M., Herz, J., Doeppner, T.R., König, R., Hütten, H., Etemire, E., Männ, L., Klingberg, A., Fischer, T., et al. (2015). Very-late-antigen-4 (VLA-4)-mediated brain invasion by neutrophils leads to interactions with microglia, increased ischemic injury and impaired behavior in experimental stroke. Acta Neuropathol. *129*, 259–277.
36. Okazaki, Y., Furuno, M., Kasukawa, T., Adachi, J., Bono, H., Kondo, S., Nikaido, I., Osato, N., Saito, R., Suzuki, H., et al.; FANTOM Consortium; RIKEN Genome Exploration Research Group Phase I & II Team (2002). Analysis of the mouse transcriptome based on functional annotation of 60,770 full-length cDNAs. Nature *420*, 563–573.
37. Chen, J., Liu, Y., Lu, S., Yin, L., Zong, C., Cui, S., Qin, D., Yang, Y., Guan, Q., Li, X., and Wang, X. (2017). The role and possible mechanism of lncRNA U90926 in modulating 3T3-L1 preadipocyte differentiation. Int. J. Obes. *41*, 299–308.
38. Xu, H., Jiang, Y., Xu, X., Su, X., Liu, Y., Ma, Y., Zhao, Y., Shen, Z., Huang, B., and Cao, X. (2019). Inducible degradation of lncRNA Sros1 promotes IFN-γ-mediated activation of innate immune responses by stabilizing Stat1 mRNA. Nat. Immunol. *20*, 1621–1630.
39. Ait-El-Mkadem, S., Dayem-Quere, M., Gusic, M., Chaussenot, A., Bannwarth, S., François, B., Genin, E.C., Fragaki, K., Volker-Touw, C.L.M., Vasnier, C., et al. (2017). Mutations in MDH2, Encoding a Krebs Cycle Enzyme, Cause Early-Onset Severe Encephalopathy. Am. J. Hum. Genet. *100*, 151–159.
40. Adrover, J.M., Del Fresno, C., Crainiciuc, G., Cuartero, M.I., Casanova-Acebes, M., Weiss, L.A., Huerga-Encabo, H., Silvestre-Roig, C., Rossaint, J., Cossío, I., et al. (2019). A Neutrophil Timer Coordinates Immune Defense and Vascular Protection. Immunity *50*, 390–402.e10.
41. Brait, V.H., Rivera, J., Broughton, B.R., Lee, S., Drummond, G.R., and Sobey, C.G. (2011). Chemokine-related gene expression in the brain following ischemic stroke: no role for CXCR2 in outcome. Brain Res. *1372*, 169–179.
42. Chen, J., Zhang, M., Zhang, X., Fan, L., Liu, P., Yu, L., Cao, X., Qiu, S., and Xu, Y. (2019). EZH2 inhibitor DZNep modulates microglial activation and protects against ischaemic brain injury after experimental stroke. Eur. J. Pharmacol. *857*, 172452.
43. Zhou, Z., Jiang, R., Yang, X., Guo, H., Fang, S., Zhang, Y., Cheng, Y., Wang, J., Yao, H., and Chao, J. (2018). circRNA Mediates Silica-Induced Macrophage Activation Via HECTD1/ZC3H12A-Dependent Ubiquitination. Theranostics *8*, 575–592.
44. Cai, W., Dai, X., Chen, J., Zhao, J., Xu, M., Zhang, L., Yang, B., Zhang, W., Rocha, M., Nakao, T., et al. (2019). STAT6/Arg1 promotes microglia/macrophage efferocytosis and inflammation resolution in stroke mice. JCI Insight *4*, e131355.
45. Shen, Q., Chen, Z., Zhao, F., Pan, S., Zhang, T., Cheng, X., Zhang, L., Zhang, S., Qi, J., Li, J., et al. (2020). Reversal of prolonged obesity-associated cerebrovascular dysfunction by inhibiting microglial Tak1. Nat. Neurosci. *23*, 832–841.
46. Wang, Y., Jin, H., Wang, W., Wang, F., and Zhao, H. (2019). Myosin1f-mediated neutrophil migration contributes to acute neuroinflammation and brain injury after stroke in mice. J. Neuroinflammation *16*, 77.
47. Deng, Y., Herbert, J.A., Smith, C.M., and Smyth, R.L. (2018). An in vitro transepithelial migration assay to evaluate the role of neutrophils in Respiratory Syncytial Virus (RSV) induced epithelial damage. Sci. Rep. *8*, 6777.
48. Tao, W., Yu, L., Shu, S., Liu, Y., Zhuang, Z., Xu, S., Bao, X., Gu, Y., Cai, F., Song, W., et al. (2021). miR-204-3p/Nox4 Mediates Memory Deficits in a Mouse Model of Alzheimer's Disease. Mol. Ther. *29*, 396–408.